# Froude-Krylov force estimation and waypoint tracking control of an underactuated model boat

Ya HUANG*
*School of Mechanical and Design Engineering*
*University of Portsmouth*
Portsmouth, UK
ya.huang@port.ac.uk

Andrea Bucchi
*School of Mechanical and Design Engineering*
*University of Portsmouth*
Portsmouth, UK
andrea.bucchi@port.ac.uk

***Abstract*—The current investigation combines the control of boat heading and speed into one logic framework using a proportional waypoint-following regulator in a surge-sway-yaw planer model based on a 1x0.55 m model boat. The proposed control logic uses the thrust angle and the thrust force as control inputs and the boat yaw angle and speed as control outputs. This control scheme is believed to be more intuitive in interpreting the human-machine interaction, and simpler in computational effort in both simulation and deployment. Three sets of hydrodynamic damping coefficients are extracted from the computational fluid dynamics (CFD) simulations assuming only the Froude-Krylov (FK) force and moment due to the incident wave without any structure obstruction. The study clarified the full hydrodynamic forces and moments required for a comprehensive simulation of fluid-structure interaction. The FK simulation results establish the benchmark that can be used to compare and demonstrate effects of different levels of hydrodynamic simplification on path following performances.**

***Keywords—proportional control, hydrodynamic drag, unmanned surface vehicle, trajectory planning, Froude-Krylov force***

## I. INTRODUCTION

The control of a surface vessel requires a different set of dynamic parameters to characterise the system in comparison to aero- and ground-vehicles. Particularly, hydrodynamic damping of a vessel plays an essential role in a path-following controller. The present study intends to demonstrate such effect using a simple proportional controller.

The overall hydrodynamic loads acting on a floating structure can be superposed by: (a) the excitation from the fluid comprised of 1) the Froude-Krylov (FK) force and moment due to the incident wave without any structure obstruction and 2) the diffraction force and moment due to the interference of a fixed structure; (b) the radiation force and moment exerted on the fluid by the movement of the structure in any of the six degrees of freedom. In the present paper the hydrodynamic drag forces related to the sway, surge and yaw motion were estimated via a commercial package for Computational Fluid Dynamics (CFD) simulation. The motion of the boat was imposed on still water and the drags were calculated as integral of the pressure distribution on the wetted surface. This simplified approach only captures the effect of the Froude-Krylov force due to the incident oncoming flow, but it does not take into account the diffraction force exerted on the fluid nor the wave oscillation frequency-dependent harmonic pressure variation due to radiation caused by the motion of the floating structure. In this study, we focus on the simplified FK hydrodynamic force in order to establish a benchmark to compare with the full hydrodynamic forces developed using a complete strip theory code to be presented in a future publication.

A basic dynamic simulation framework to identify design parameters of unmanned surface vehicles (USV) in surge, sway and yaw axes is improved in the present paper from its predecessor [1] in the MATLAB-Simulink® environment. The present paper describes 1) a multiple fixed waypoint updating framework using the same motion control algorithm developed in [1]; 2) effects of hydrodynamic damping coefficient of vessel hull forms derived from a set of CFD simulations [2]. The study provides small USV designers a starting point for their guidance navigation and control (GNC) system, and some practical considerations on selecting material to construct the surface vehicle as a mechanical system.

The motion control component in the GNC system [3] is to determine the necessary control forces and moments to execute specific control objectives provided by the guidance system which involves the generation of an optimal path. In the present study, path-following control is used to demonstrate the control performance using a set of predefined waypoints (forming a path) independent of time. For fundamentals of controller designs, simulation and implementation for surface vessels, the readers are referred to [3] and [4] starting from theories of open-loop control and close-loop Proportional-Integral-Derivative (PID) control laws. For more advanced nonlinear and hybrid control methods, readers are directed to an update-to-date review study [5]. Among them, fuzzy membership functions were shown to mimic experienced helmsman for local path planning with obstacles [6]. Several variants of A* algorithms, e.g. Rule-based Repairing A* (R-RA*), can detect and avoid multiple 'pop-up' moving obstacles in compliance with the International Regulations for Preventing Collisions at Sea 1972 (COLREGs) for local replanning with fast real-time solution independent of vessel communication data [7]. However, vessel dynamics and speed were not considered. Artificial Potential Field (APF) methods have been demonstrated to account for the unpredictable strategies of obstacle vessels with a smoother path considering the dynamics of obstacles. But the vessel speed reduction was not implemented at manoeuvring points, neither were environmental disturbance uncertainties [8]. A path-guided hybrid APF was able to tackle local minima, an inheriting problem with conventional APF methods, oscillations in narrow passages and "goals non-reachable with obstacles nearby" problems but only as a local path adjustment algorithm [9]. Model Predictive Control (MPC) makes use of numerical optimization to select receding future 'horizons' of paths and states, but complex collision avoidance scenarios could

* Correspondence author: Ya Huang ( ya.huang@port.ac.uk )

lead to non-convex optimization formulations exhibiting local minima. A solution to the gradient-descent optimisation problem is to select a finite number of control contours based on their cost and feasibility [10]. Such optimisation approach is able to take into account vessel dynamics, heading and speed, environmental disturbance forces, and multiple obstacles. More recently, reinforcement learning, e.g. Q-learning, exploited self-learning and continuous optimisation close to human manoeuvring and guaranteed that a rational path is always found [11].

The majority of the advanced control methods reviewed have been based on the specific path planning algorithm and optimisation techniques adopted. While one may argue these higher levels of 'controls' may be well placed in the territory of path planning and navigation, the focus of the present study is to isolate the 'lower' level control problem when the paths or waypoints have already been decided or continuously updated.

The present study applies the most basic forms of control, i.e., the proportional control. Control systems can be simple with straightforward mathematical expressions to achieve the control objectives, e.g. heading angle and distance to the next waypoint. The outcome is satisfactory only if the vessel's inertia properties, i.e. mass, mass moment of inertia, and product moment of inertia, are small, and accurate trajectory is not required. Minorsky (1922) developed the PID control law that requires tuning of the three respective gains [4, 12]. Usually a proportional-derivative (PD) controller is adequate for underactuated vessels, i.e. the number of control inputs is less than the generalised coordinates or degrees of freedom – surge, sway and yaw in the present case [3], to regulate the heading or yaw angle. The present investigation proposes to use only proportional control principles in the simulation, considering: the vessel size, hydrodynamic damping, vessel speed, path characteristics, and environmental disturbances. The high proportional gain in a PID controller produces a faster response and smaller residual error over time, but at the cost of overshooting and oscillation; a high derivative gain can reduce the overshooting acting just like analogue damping to smooth out oscillations and overshooting in the response. The hydrodynamic damping or drag coefficient can play the same role as a derivative gain in the PID controller, reducing the complexity of the control logic with imbedded 'smoothening' effect in the system's dynamics.

A usual practice in vessel motion control is to separate controls for heading and speed [3]. The current investigation combines the control of the two aspects into one logic framework using a proportional waypoint-following regulator in a surge-sway-yaw planer model. The proposed control logic uses the thrust angle and the thrust force as control inputs and the boat yaw angle and speed as control outputs. This control scheme is believed to be more intuitive in interpreting the human-machine interaction, and simpler in computational effort in both simulation and future deployment. Different sets of hydrodynamic damping coefficients extracted from the CFD simulations [2] of a small robotic boat Pytheas built at the University of Portsmouth have been used to demonstrate the effect of damping on path following performances.

## II. METHODOLOGY

To make it easy to understand, an adapted version of the dynamics and control logic originally presented in [1] is briefly introduced in this section. Before that, the CFD simulation workflow is summarized to provide a holistic picture of how to extract hydrodynamic coefficients for different hull designs and to evaluate different fluidic parameters to configure the simulation environment [2]. All simulations were performed using MATLAB® 2019b, and all codes are provided in a GitHub repository open to all public (https://github.com/huangya17/2021-boat-control-damping).

### *A. Dynamics simulation using CFD drag coefficients*

Hydrodynamic drag forces were obtained in the surge, sway and yaw axes in the CFD simulation based on the configuration of the physical parameters defined in Table 1. The simulations were set up according to the International Towing Tank Conference (ITTC) recommended procedures and guidelines for ship CFD [13]. The computational mesh consists of approximately 3.2 million trimmed mesh cells for grid independence. The volume of fluid (VOF) solver with a flat wave model is used to capture the water surface and wave damping, preventing wave reflection. The κ-ε turbulence model was used to model the turbulence, and an implicit unsteady solver with a time step of 0.01 s was employed to extract the main flow features. From Fig 1, the linear and exponential coefficients of each of the three axes are fitted: for drag forces in the surge axis $F_x$, $d_1 = 6.7$, $a_1 = 2.2$; for drag forces in the sway axis $F_y$, $d_2 = 22.1$, $a_2 = 1.5$; for drag moments in the yaw axis $M_z$, $d_3 = 2.9$, $a_3 = 1.5$. These will be used to configure the equations of motion for the boat.

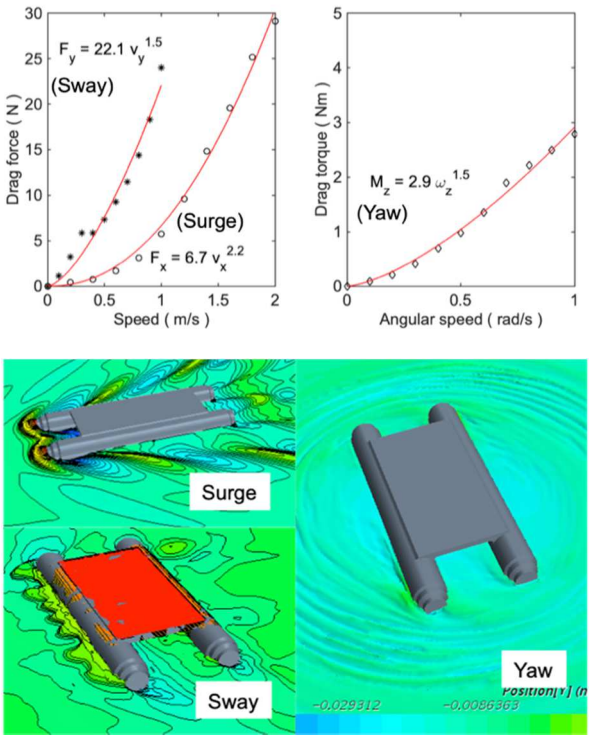


Fig 1 Hydrodynamic drag coefficients from CFD

*B. Kinematics and kinetics of boat model*

The dynamic boat model considers 2-Dimensional plane motion with three degrees of freedom (3DoF) in the body-fixed coordinate frame of x (surge) and y (sway) for translation, and z (yaw) for rotation of the boat body in the global inertia frame of XYZ.

The actual propulsion and steering system was configured according to Fig 2a, but in the simulation study this system is simplified to represent a servo steered motor producing a variable thrust force $F$ and a variable thrust angle $b$ (Fig 2b). It is assumed that disturbances from a combination of wave, current and wind could be represented by a force $F_d$ as a function of time applied at angle $k$ in the three equations of motion (Fig 2b).

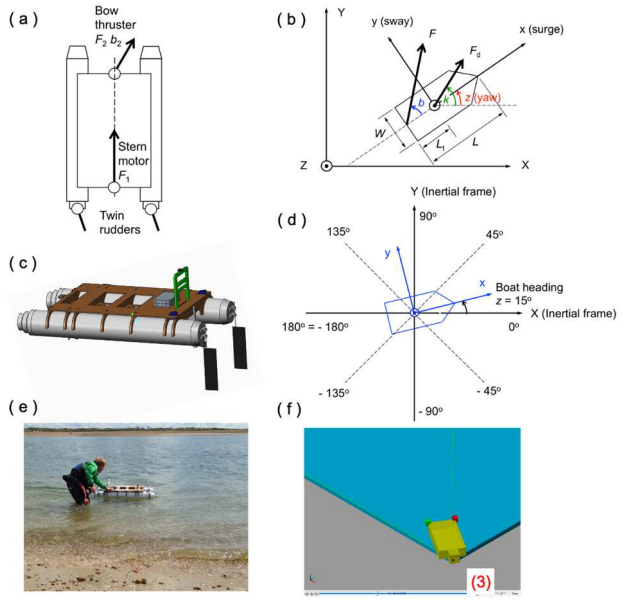


Fig 2 Schematics showing the thrust configuration (a), simplified free-body diagrams based on one vectored thruster (b), relative size of the rudder and hull (c), heading angle and coordinate systems in the simulation (d), actual boat at launch (e), and a simulation animation screenshot at waypoint 3 (f) of the Pytheas robotic boat project at University of Portsmouth.

The kinematic relationship between the boat position in the global inertial frame $XYZ$ and the boat body-fixed frame $xyz$ can be defined according to Fig 2b, d.

$$[X] = [x]\cos[z] - [y]\sin[z] \quad (1)$$

$$[Y] = [y]\cos[z] + [x]\sin[z] \quad (2)$$

$$[Z] = [z] \quad (3)$$

where $[X]$ and $[Y]$ represent translational position ($X$, $Y$), velocity ($X'$, $Y'$) or acceleration ($X''$, $Y''$) in the global inertial frame; $[x]$ and $[y]$ denote translational position ($x$, $y$), velocity ($x'$, $y'$) or acceleration ($x''$, $y''$) in the local body-fixed frame attached to mass centre of the boat; $[z]$ comprises the yaw angle ($z$), yaw angular velocity ($z'$), or yaw angular acceleration ($z''$). $[Z]$ and $[z]$ both measure yaw and are identical in both reference frames, and therefore $z$, $z'$ and $z''$ are used throughout to express any rotation or yaw.

Using the general Newton's Second Law $\sum F = ma$ and $\sum M = I\alpha$, where $\sum F$ and $\sum M$ are external forces and moments and $a$ and $\alpha$ are linear and angular accelerations, the equations of motion expressed in the local $xyz$ frame [3, 14]:

$$F\cdot\cos(b) + F_d\cdot\cos(k-z) + (m+m_{yy})\cdot y'\cdot z' - d_1\cdot\mathrm{sign}(x')\cdot|x'|^{a_1} = (m+m_{xx})\cdot x'' \quad (4)$$

$$F\cdot\sin(b) + F_d\cdot\sin(k-z) - (m+m_{xx})\cdot x'\cdot z' - d_2\cdot\mathrm{sign}(y')\cdot|y'|^{a_2} = (m+m_{yy})\cdot y'' \quad (5)$$

$$L_t\cdot F\cdot\sin(b) - (m_{yy}-m_{xx})\cdot x'\cdot y' - d_3\cdot\mathrm{sign}(z')\cdot|z'|^{a_3} = (I+I_{zz})\cdot z'' \quad (6)$$

TABLE 1 Boat parameters

| | Value | Definition |
|---|---|---|
| $L$ | 1 m | Overall length of boat |
| $L_t$ | 0.4 m | Distance between mass centre and point of action of thrust force |
| $W$ | 0.55 m | Width of boat |
| $m$ | 7 kg | Overall mass of boat |
| $m_{xx}$ | ( $r\,m$ ) kg | Added mass in surge x-axis of boat [14, 15], $r$ = [0.01, 0.05] |
| $m_{yy}$ | ($\rho\,\pi\,D^2\,L$ / 2) kg | Added mass in sway y-axis of boat [14, 15], $\rho$ = 1000 kg/m$^3$ water density |
| $I$ | ( $m(W^2 + L^2)$ / 12 ) kg m$^2$ | Mass moment of inertia of boat about mass centre in yaw z-axis |
| $I_{zz}$ | ($0.1\,m\,W^2 + p\,\pi\,D^2\,L^3$) / 2 / 12 kg m$^2$ | Linear coefficient of added mass moment of inertia in z-axis [14, 15] |
| $d_1$ | 6.7 | Hydrodynamic damping coefficient of surge x-axis (Fig 1) |
| $d_2$ | 22.1 | Hydrodynamic damping coefficient of sway y-axis (Fig 1) |
| $d_3$ | 2.9 | Hydrodynamic damping coefficient of yaw z-axis (Fig 1) |
| $a_1$ | 2.2 | Exponential damping coefficient of surge x-axis (Fig 1) |
| $a_2$ | 1.5 | Exponential damping coefficient of sway y-axis (Fig 1) |
| $a_3$ | 1.5 | Exponential damping coefficient of yaw z-axis (Fig 1) |

The geometric and inertia parameters in the above equations are summarised in Table 1. These are based on a budget catamaran test boat built with two PVC ducts, acrylic blocks and varnished Medium-Density Fibreboards (MDFs). The kinematic and kinetic variables are listed in Table 2. The range for thrust angle $b$ is determined by the servo and thrust force $F$ produced by the brushless motor.

The values for nonlinear hydrodynamic damping coefficients ($d_1$, $d_2$, $d_3$, $a_1$, $a_2$, $a_3$) in equations (4)-(6) are estimated based on the force-velocity relationships of the CFD simulation – see Fig 1. The values obtained in Section 1 and Table 2 were based on the configuration of the boat without any tracking rudders seen in Fig 2c. These coefficients depend largely on the hull form, size and speed of the boat. The units for $d_i$ and $a_i$ (i = 1, 2, 3) are SI standard to give rise to N for $(d_i \cdot \text{sign}(x') \cdot |x'|^{a_i})$.

The uniform disturbance force $F_d$ is modelled as a sinusoidal time function of long-crested wave acting solely at the mass centre of the boat [8].

$$F_d = A \sin(w_d\, t) + B \qquad (7)$$

where $A$ is the amplitude of the disturbance force (N), $w_d$ is the oscillatory frequency of the disturbance force (rad), $B$ is the bias – the constant component of force that applies (N), $t$ is time (s). Usually $A \leq B$. For the present simulation, the following disturbance parameters are fixed: A = 10 N, B = 10 N, $w_d$ = 0.628 rad/s or 0.1 Hz. The angle of attack of the disturbance force $k = \pi/4$ (Fig 2b). These parameters represent the combined effect of any disturbances from environment, e.g. current and wind loads.

The boat heading $z$ and disturbance force angle $k$ are both measured relative to the +X of the global inertial frame, while the thrust angle $b$ is measured relative to the +x of local fixed-body frame (see Fig 2b, d). The thrust force $F$ and thrust angle $b$ are determined using a logic control to follow the heading angle demand for the position of the next waypoint.

The dynamic relations and control algorithms are simulated using MATLAB-Simulink® (2019b). The three equations of motion (4 – 6) are integrated using a Runge–Kutta fourth order integrator.

TABLE 2 Kinematic and kinetic variables

| | Unit | Definition |
|---|---|---|
| $x$, $x'$, $x''$ | m, m/s, m/s$^2$ | Current boat position, velocity, acceleration in local x-axis (surge) |
| $y$, $y'$, $y''$ | m, m/s, m/s$^2$ | Current boat position, velocity, acceleration in local y-axis (sway) |
| $z$ | rad | Current boat heading relative to +X of inertial frame [-π, π], yaw |
| $z'$, $z''$ | rad/s, rad/s$^2$ | Boat heading angular velocity and angular acceleration |
| $b_{max}$ | 0.47π rad | Maximum thrust angle |
| $b$ | rad | Thrust angle relative to boat heading +x of local frame [-$b_{max}$, $b_{max}$] |
| $k$ | rad | Disturbance force angle relative to +X of inertial frame [-π, π] |
| $F_{max}$ | 20 N | Maximum thrust force |
| $F$ | N | Thrust force [0, $F_{max}$] |
| $F_d$ | N | Disturbance force acting at mass centre assuming long-crested wave [3] |

*C. Control logic*

The pseudo code of six steps to derive the control inputs – thrust force $F$ and thrust angle $b$ in order to reach the next waypoint is presented along with the main control objectives: heading angle difference between demand and current heading, and the distance to the next waypoint. The speed of the boat is not included as the control objective as the maximum surge speed is under 1.5 m/s. See Appendix I for the controller implemented using MATLAB function 'nav(.)' as part of the Simulink model with an overview presented in Fig 3. The six steps of the full control logic are summarized below.

1) Obtain next waypoint ($X_w$, $Y_w$), current position ($X$, $Y$), heading ($z$), max thrust force $F_{max}$ and thrust angle $b_{max}$.

2) Compute demand heading:

$hd$ = atan2( $(Y_w - Y)$ / $(X_w - X)$ ), where 'atan2(.)' returns four-quadrant inverse tangent in the range [-π, π];

current distance to next waypoint:

$dst = \sqrt{(Y_w - Y)^2 + (X_w - X)^2}$

heading difference between demand and current heading:

$dhd = hd - z$

3) Ensure heading difference $dhd$ is in range [-π, π].

if $dhd < -\pi$
    $dhd = 2\pi + dhd$
elseif $dhd > \pi$
    $dhd = -2\pi + dhd$

4) Check if distance to next waypoint $dst$ is less than $wp\_tol$.

if $dst <= wp\_tol$
    stop ($F = 0$, $b = 0$) or update waypoint
else
    go to step 5)

5) Determine the direction to turn.

# for small turning angle

if ($dhd > -\pi/2$) and ($dhd < \pi/2$):

    $b = b_{max}\, dhd / (\pi/2)$  # proportional to $dhd$
    $F = F_{max}$  # max thrust

# for large turning angles
elseif ( ( $dhd >= -\pi$ ) and ( $dhd <= -\pi/2$ ) ) or
    ( ( $dhd >= \pi/2$ ) and ( $dhd <= \pi$ ) ):
    $b = b_{max}$ ( sign($dhd$) )  # max thrust angle to turn

    if $dst <= wp\_sh$:

$F = (F_{max}/3)$ $(dst/\ wp\_sh)$ # reduced thrust

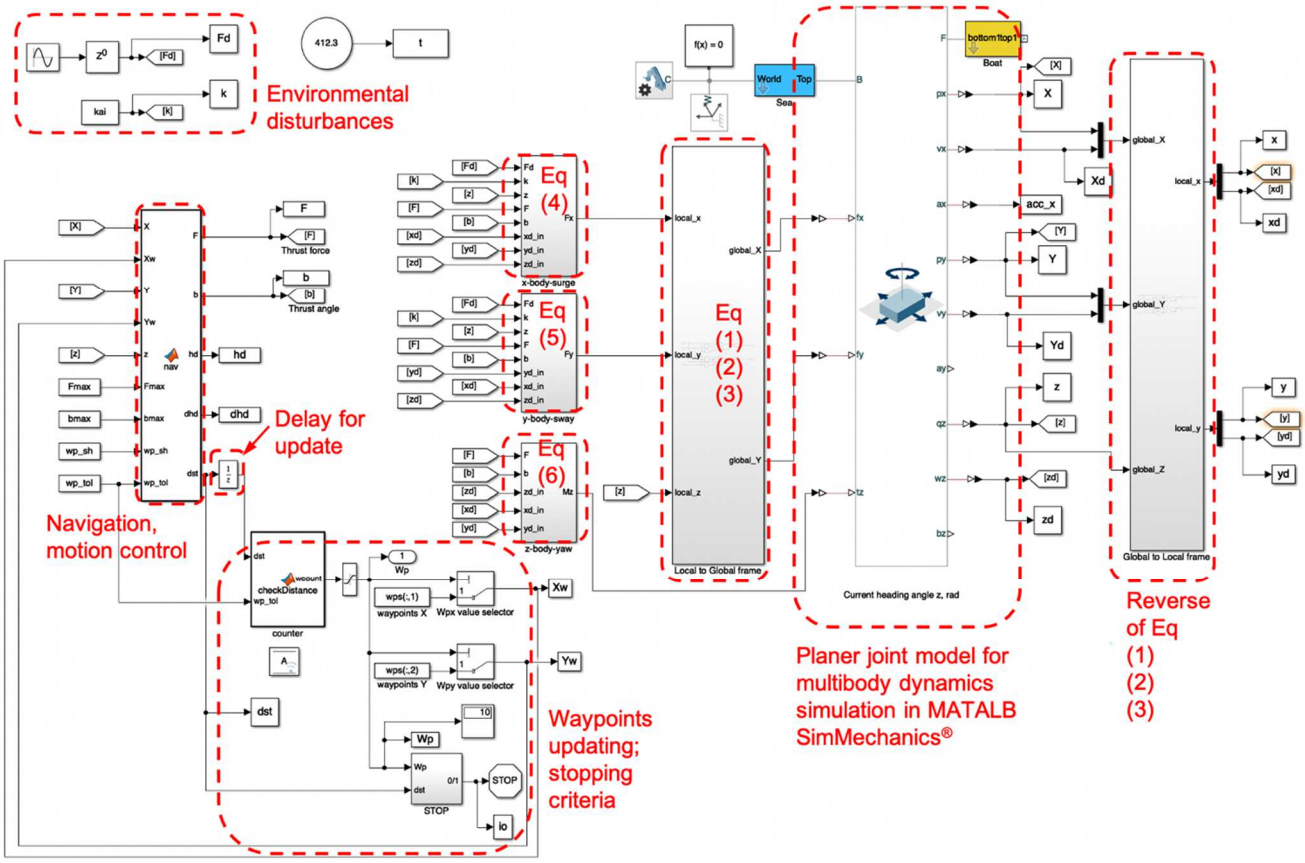


when close to waypoint

else:

$F = F_{max}/2$ # half thrust for large turning angle

6) Two function blocks of 'Delay for update' and 'Waypoints updating; stopping criteria' have been added to the original model adopted from [1] to allow the simulation to continue once the waypoint is reached. The variable *wp_sh* above is the 'short distance' criteria used to slow down the boat when it is close to the waypoint, e.g. *wp_sh* = 10 m, but before reaching it.

Fig 3 The simulation architecture implemented in MATLAB-Simulink: navigation and motion control, boat dynamics module using Eq (1 – 6) where *xd* = *x*' and *xdd* = *x*", waypoint updating, and disturbances.

At each integration step, the above control algorithm updates its current boat (mass centre) position in the global inertial frame (*X*, *Y*) in step 1), and computes the heading difference *dhd* and distance to the waypoint *dst* in step 2). Step 3) ensures the heading difference *dhd* to be in the range [-π, π], so as to prevent swirling. Step 4) sets the tolerance for reaching a waypoint *wp_tol*. A distance of *wp_tol* = 1 m is considered accurate for a boat of one metre long and half a metre wide in the simulation study.

Step 5) is the main iterative step of boat control before reaching the waypoint tolerance *wp_tol*. First, the turns are classified as 'small turn' with heading difference *dhd* in the range (-π/2, π/2) and 'large turn' with heading difference *dhd* in [-π, -π/2] or [π/2, π]. In the case of a small turn (less than π/2 either side), thrust angle *b* is proportional to heading difference *dhd* with a fixed gain of $b_{max}/(\pi/2)$; thrust force *F* is set to maximum $F_{max}$. In the case of a large turn (between π/2 and π either side), thrust angle *b* is set to maximum $b_{max}$. But the thrust force *F* is adjusted according to the current distance to waypoint *dst*. If this distance is less than *wp_sh* = 10 m, the thrust force *F* is reduced in proportion to *dst* by multiplying $(F_{max}/3)$ with $(dst/\ wp\_sh)$. If the distance is greater than *wp_sh*, the thrust force is limited to a half of the maximum. To experience, the reduced thrust force provides a better chance for the boat to reach the waypoint at large turns between π/2 and π at close proximity. As a rule of thumb, a distance range for *wp_sh* between 10 and 20 m seems to give a good heading control based on the specification of the current boat: $F_{max}$, $b_{max}$, mass moment of inertia, length, width, hydrodynamic damping coefficients to turn. These factors affect the boat forward speed and maximum turning moment that dominate the behaviour of the boat when approaching the radius tolerance of the waypoint *wp_tol* = 1 m. The actual behaviour would inevitably be influenced and complicated by the direction (*k*) and magnitude of the disturbance force $F_d$.

## III. Results and Analysis

The simulated boat starts from rest at the global inertial frame origin (0, 0) with an initial heading angle in the +*X* direction. All waypoints are defined in the global inertial frame by (*X*, *Y*). The simulation is terminated once the boat

reaches all 9 waypoints (Fig 4b). The waypoints from (1) to (9) were designed to examine the manoeuvrability derived as a simpler version of the Kempf's zigzag manoeuvre [3] for quadrants of the global frame.

The results are presented to compare three sets of hydrodynamic damping configurations shown in Table 3. Each of the six parameters for configuration *C1* has been elaborated in Section 2.1 and Table 1. *C2* sees increased values in each of the six parameters – these are based on estimation of adding the pair of tracking rudders at the stern of the robotic boat depicted in Fig 2c. *C3* has a further increase in each of the six damping coefficients representing increased hydrodynamic interactions and features such as additional underwater instruments. It is hypothesised that better tracking behaviour provided by the rudders will provide higher hydrodynamic damping giving rise to the equivalent effect of the increased derivative control gain in a PID controller. This would increase the stability at each manoeuvring (way)point with less oscillatory response and less overshooting. The increase in $d_1$ is less comparing to $d_2$ and $d_3$ as the latter two represents the sway and yaw linear damping coefficients which are influenced by the added tracking rudders to a greater extend.

TABLE 3 Three hydrodynamic damping configurations from Eq (4 - 6)

| | $d_1$ | $d_2$ | $d_3$ | $a_1$ | $a2$ | $a_3$ |
|---|---|---|---|---|---|---|
| *C1** | 6.7 | 22.1 | 2.9 | 2.2 | 1.5 | 1.5 |
| *C2* | 8 | 50 | 6 | 3 | 2 | 2 |
| *C3* | 10 | 60 | 9 | 3 | 2 | 2 |

**C1* is derived from the CFD workflow in Section 2.1.

The time histories of distance to the 'next waypoint' (*dst*) offers the first impression of the waypoint tracking performance at each of the 9 waypoints without (Fig 4a) and with the disturbance force $F_d$ (Fig 5a). With no disturbance force, the fluctuation shown in the straight-line part of the trajectory map (Fig 4b) and the angle and speed time histories (Fig 6a, c) suggest an approximate oscillation frequency of 0.16 Hz, i.e. 16 oscillations in 100 s, most obvious in Fig 6a. This is the natural oscillation frequency dictated by the boat-fluid hydrodynamics and the controller. Adding the predefined disturbance force, the main oscillation frequency is governed by the driving frequency of the disturbance force which is 0.1 Hz. This behaviour is consistent with a second order dynamic system where the restoring force is represented by a spring component and the damping force by a viscous damper. When there is no disturbance force, the system shows its natural frequency during 'free' vibration; with imposed disturbance driving force, the system response frequency is the same as the driving frequency.

As the hydrodynamic damping coefficients increases from *C1* to *C3*, the boat takes noticeably more time to reach each waypoint, but with less fluctuations – both observable in the *dst* (Fig 4a) and in the trajectory map (Fig 4b) without and with disturbance force (Fig 5a, b). It is worth noting that the sinusoidal disturbance force $F_d$ defined by Eq (7) is constantly applied at an angle ($k$) of $\pi/4$ from the +X inertial frame. Given that the sum of the amplitude of the sinusoidal disturbance force $A$ = 10 N and the constant offset $B$ = 10 N is 20 N which matches the maximum of thrust force $F_{max}$ = 20 N, the boat is able to reach all waypoints. The same is true when the disturbance angle $k$ is changed to all four quadrants of the inertial frame, e.g. $-\pi/4$, $\pm\pi/2$, $\pm 3\pi/4$, and $\pi$. But only the results $k = \pi/4$ is presented with disturbance force.

Using the hydrodynamic damping configuration *C3* as an example, the boat heading angle $z$ in the first 300 s confirms the 5 waypoints, i.e (2) to (6), reached at different stages with corresponding actions from the thrust angle $b$ (Fig 6a, 7a). The three velocity components in surge, sway and yaw illustrate the 2D motion of the boat at any instance (Fig 6c, 7c) with the variation of yaw velocity matching the thrust angle $b$ in Fig 6a and 7a. The maximum thrust force $F_{max}$ = 20 N matches the peak disturbance force $F_d$ (Fig 7d). With no disturbance force, Fig 6d shows three occasions before reaching waypoint (7) (before 300 s) when the thrust force $F$ is dropped by half due to passing waypoints (2) around 56 s, (3) around 137 s, and (6) around 233 s. This is caused by the control logic detecting a large turning angle demand more than $\pi/2$ (see Step 5 of Section 2.3). With the disturbance force, Fig 7d shows four occasions before reaching waypoint (7) (before 300 s) when the thrust force $F$ is dropped by half due to passing waypoints (2) around 79 s, (3) around 153 s, (4) around 183 s, and (6) around 246 s. The drop in thrust force approaching waypoint (4) is caused by a drift of the boat trajectory away from the straight-line path between waypoints (3) and (4). This in turn triggers the control logic to detect a large turning angle demand more than $\pi/2$.

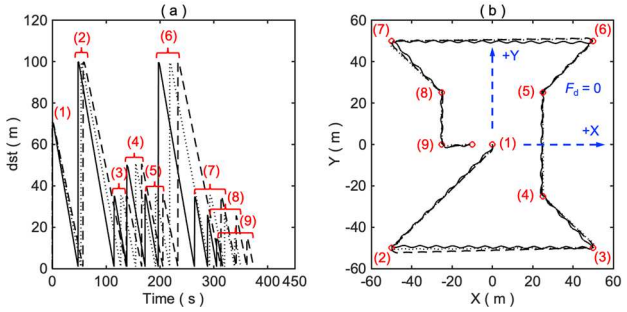


Fig 4 Times histories of the distance to each of the 9 waypoints (*dst*) (a), and full trajectories (b) using the three damping configurations – solid lines (__) for *C1*, dotted lines (…) for *C2*, and broken lines (- - -) for *C3* – with disturbance force $F_d$ = 0 of Eq (7).

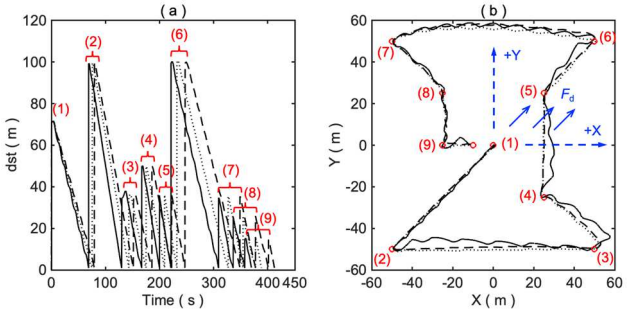


Fig 5 Times histories of the distance to each of the 9 waypoints (*dst*) (a), and full trajectories (b) using the three damping configurations – solid lines (__) for *C1*, dotted

lines (…) for *C2*, and broken lines (- - -) for *C3* – with disturbance force $F_d = 10\sin(0.628t)+10$ of Eq (7).

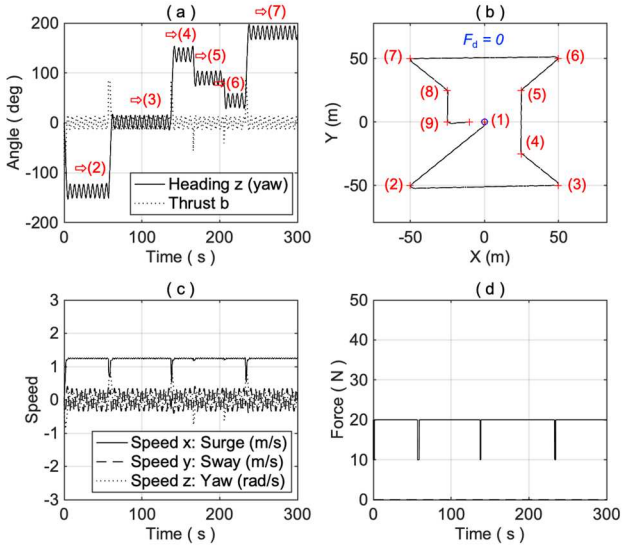


Fig 6 Angle (a), trajectory (b), speed (c) and thrust force *F* (d) time histories showing the approaching to the 9 waypoints using hydrodynamic damping configuration *C3* with disturbance force $F_d = 0$ of Eq (7).

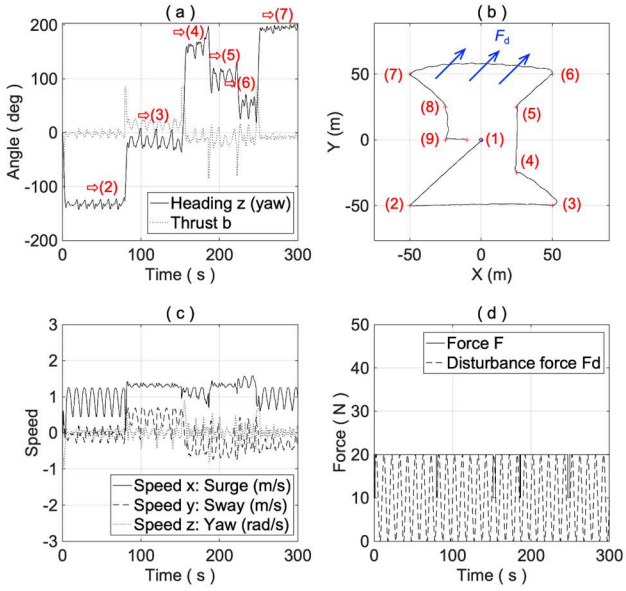


Fig 7 Angle (a), trajectory (b), speed (c) and force (d) time histories showing the approaching to the 9 waypoints using hydrodynamic damping configuration *C3* with disturbance force $F_d = 10\sin(0.628t)+10$ of Eq (7).

As the hydrodynamic damping coefficient increases from *C1* to *C3*, the boat exhibits a more stable turning trajectory at the waypoint (3) and the regulation of boat velocity vector becomes more effective (Fig 8). Waypoint (3) is selected to plot the detailed quiver vector-trajectory time histories in Fig 8, as after the turn, the disturbance force $F_d$ will be approximately at $-\pi/2$ to the boat demand heading – the most demanding condition for maintaining directional stability until reaching the next waypoint. While increasing damping from *C1* to *C2* improves the trajectory of turning with reduced fluctuation (Fig 8a, b), the increase of damping from *C2* to *C3* results in more sway after the turn (Fig 8c). In the hydrodynamic design of the hull form, more control surfaces such as the tracking rudder pair or skegs, represented by increased damping, would provide more tracking at a manoeuvring waypoint. But the path tracking performance is largely influenced by the changing disturbance force and its direction.

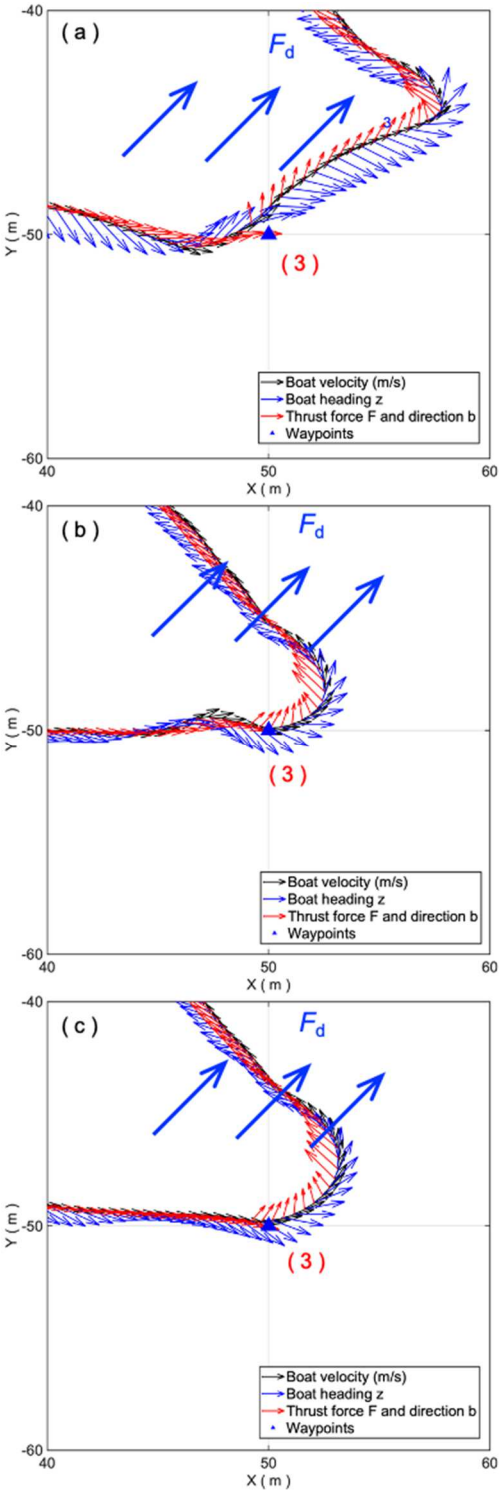


Fig 8 Vector boat velocity, boat heading and thrust force over-laid on the trajectories around waypoint (3) for hydrodynamic damping configurations *C1* (a), *C2* (b) and

*C3* (c) with disturbance force $F_d = 10 \sin(0.628t) + 10$ of Eq (7).

## IV. Discussion and Conclusions

This section remarks on the main limitations and outcomes of the presented work and discusses any implications on the controller design and implementation on real systems.

For large ship and ocean crossing vessels, three degrees-of-freedom planer model of surge, sway and yaw is adequate in most conditions when environmental disturbance forces are less than the inertial and propulsion forces [3]. The three axes also form the main axes of motion control objectives, i.e. where the vessel moves in the 2D plane of the ocean. To minimise the computational effort and to pursue the same motion control objectives, the present study adopts this approach. In reality, pitch, roll and heave motions are closely coupled with the planer model, especially when external disturbance force in all six degrees of freedom matches the magnitude of thrust force. This could well be the case when the robotic boat is small (Pytheas: 1 x 0.55 m, 7 kg, maximum thrust 20 N). There would be overwhelmingly large disturbance force in all six axes and constantly changing. A conservative controller designer would argue that the 3-DoF planer model simulation would provide little insight to the actual controller performance of a small robotic boat in the open ocean. On the other hand, in reality, the combined effect of constantly changing disturbance force (both its magnitude and direction) in all six axes may be in favour of the control objectives from time to time, providing an overall advantage for the journey. As an underactuated system, the boat has two control outputs – the thrust force and angle, and there are six degrees of freedom of movement and disturbance. If the path planning can take into account of the varying disturbance force, the simulation will be able to predict, to an extent, that whether the path can be achieved despite the complexity of the model with 3-DoF or 6-DoF. On a sunny day of sea states 1-2 (30th April 2016), the student project Pytheas robotic boat crossed between the Southsea Langstone campus to Haling Island, a stretch of 0.5 km of open channel (https://youtu.be/qwa65KnJfJ0). The boat returned and stopped at the finishing waypoint within less than 10 m diameter after a 1.1 km journey.

One dominant disturbance model is the surface wave magnitude and direction of propagation. The oceanography community has established the stereo imaging technique to extract wave and wind dynamics from the imaging data [16]. In order to provide usable information for local close-proximity boat control, the general sea state rating has little value to add. Instead, the semantic surface wave observational model derived from the imaging data can be used to develop an accurate disturbance force model using CFD simulation to map the surface wave observation to dynamic loads acting on the vessel. However there has been no known work to address this gap so far. Such a hybrid observational model of the disturbance would influence designs of the boat hydrodynamics and the controller.

The current study demonstrates the effectiveness of increased hydrodynamic damping using added fluid-structure control surfaces such as tracking rudders and skegs in enhancing tracking performance of the boat with less fluctuation and overshooting at manoeuvring waypoints. However, the investigation is restricted to the simplest form of thrust force configuration, i.e. a single variable thruster force acting at the stern of the boat. In a previous study [1], different propulsion system configurations (of rudders, motors, servos, and 'azipods') were provided. From a robotic boat designer's point of view, a lot of what-if questions of various designs can be answered using the simulation framework, including: the maximum thrust force required, the range of the thrust force angle, the number of thrusters required, and the most important of all, the hull form and hydrodynamic features to improve the tracking and manoeuvrability of the boat. These will all affect the hydrodynamic damping and therefore control response.

The simulation framework provides a multiple-waypoints simulation environment in 2D incorporating 3-DoF. The next step is to combine multiple obstacle avoidance and path planning algorithms developed in a predecessor of the present study using an iterative trigonometric algorithm to optimise the path avoiding multiple obstacles between waypoints [2].

In our future work, via the strip theory the excitation force can be evaluated as combination of the incident wave contribution from the Froude-Krylov force and the scattering wave while the structure is artificially hold still. The excitation force will permit the solution of the ship motion under the action of gravity water waves.

In order to solve the radiation problem due to structure movement in the fluid, the equation of motions require the definition of added mass and fluid damping coefficients for each degree of freedom of interest. The evaluation of such coefficients can also be accommodated by a strip theory approach. As a result, the ship will experience a harmonic response at the incident wave (encounter) frequency in all the degrees of freedom except in surge which holds a constant speed by definition. The harmonic motion will be reflected in fluctuating velocities in the associated degrees of freedom. These velocities can be used then to estimate a more comprehensive hydrodynamic drag forces and movements via the classical formula $D = \frac{1}{2} C_D \rho V^2 S$ where $C_D$ is drag coefficient, $\rho$ is fluid density, $V$ is relative speed between fluid and body, $S$ is the cross-sectional area in the frontal view of the wetted body. The coefficient of drag is also related to the geometric shape of the wetted body.

The proposed strip theory framework will allow researchers to have full control of how the hydrodynamic effects are modelled and simulated in order to accommodate a wide range of operational conditions against simulation results from commercial packages.

## Appendix I Control logic in MATLAB script

The navigation controller to find thrust force $F$ and thrust angle $b$ in order to reach the next waypoint implemented in a MATLAB function 'nav' in the Simulink model (Fig 3).

```
Function [F,b,hd,dst] =
nav(X,Xw,Y,Yw,z,xd,Fmax,bmax)

Xdiff = Xw - X ;
```

```
Ydiff = Yw - Y ;
dst = sqrt(Xdiff^2 + Ydiff^2) ;

hd = atan2(Ydiff,Xdiff) ;
dhd = hd - z ;

F = 0 ;
b = 0 ;

if dhd < -pi
    dhd = 2*pi + dhd ;
elseif dhd > pi
    dhd = -2*pi + dhd ;
end

if (dst <= wp_tol)
    F = 0 ;
    b = 0 ;
else
    if (dhd > -pi/2) && (dhd < pi/2)
        b = bmax*dhd/(pi/2) ;
        F = Fmax ;
    elseif ((dhd >= -pi)&&(dhd <= -pi/2)) ||
((dhd >= pi/2)&&(dhd <= pi))
        b = bmax*(sign(dhd)) ;
        if (dst <= wp_sh)
            F = (Fmax/3)*(dst/ wp_sh) ;
        else
            F = Fmax/2 ;
        end
    end
end
```

## REFERENCES


[1] Y Huang, Z Ji (2017). Autonomous boat dynamics: how far away is simulation from the high sea? IEEE Proceedings of OCEANS, Aberdeen, p2106-2113.

[2] D Stergianelis, Y Huang, M McConnell, H Yu, Z Ji (2020). A simulation study of simple local path planning and control for unmanned surface vehicles. IEEE Proceedings of OCEANS, Singapore. Xplore 978-1-7281-5446-6/20.

[3] TI Fossen (2011). Handbook of marine craft hydrodynamics and motion control. Chichester, UK: John Wiley&Sons Ltd.

[4] CS Chin (2013). Computer-Aided Control Systems Design: practical applications using MATLAB and Simulink. Taylor&Francis Group.

[5] A Vagale, R Oucheikh, RT Bye, OL Osen (2021). Path Planning and Collision Avoidance for Autonomous Surface Vehicles II: A Review. Journal of Marine Science and Technology.

[6] L Perera, J Carvalho, C Soares (2010). Autonomous guid- ance and navigation based on the COLREGs rules and reg- ulations of collision avoidance. In Advanced Ship Design for Pollution Prevention. Taylor & Francis Group.

[7] S Campbell, M Abu-Tair, W Naeem (2014). An automatic COLREGs-compliant obstacle avoidance system for an un- manned surface vehicle. Proceedings of the Institution of Mechanical Engineers Part M: Journal of Engineering for the Maritime Environment, 228(2) p108–121.

[8] W Naeem, SC Henrique, L Hu (2016). A Reac- tive COLREGs-Compliant Navigation Strategy for Au- tonomous Maritime Navigation. IFAC.

[9] H Lyu, Y Yin (2018). Fast path planning for autonomous ships in restricted waters. Applied Sciences (Switzerland), 8(12) p6–8.

[10] TA Johansen, T Perez, A Cristofaro (2016). Avoidance and COLREGS Compliance Using Simulation- Based Control Behavior Selection With Predictive Hazard Assessment. IEEE Transactions on Intelligent Transportation Systems, 17(12) p3407-3422.

[11] C Chen, XQ Chen, F Ma, XJ Zeng, J Wang (2019). A knowledge-free path planning approach for smart ships based on reinforcement learning. Ocean Engineering 189.

[12] N Minorsky (1922). Directional stability of automatically steered bodies. Journal of the American Society for Naval Engineers 34 p280-309

[13] ITTC Recommended Procedures and Guidelines (2011). Practical Guidelines for Ship CFD Applications 7.5-03-02-03.

[14] KR Muske, H Ashrafiuon, G Haas, R McCloskey, T Flynn (2008). Identification of a control oriented nonlinear dynamic USV model, American Control Conference, Seattle WA, p562-567.

[15] JN Newman (1977). Marine hydrodynamics. MIT Press.

[16] F Bergamasco, A Torsello, M Sclavo, F Barbariol, A Benetazzo (2017). WASS: An open-source pipeline for 3D stereo reconstruction of ocean waves. Computers & Geosciences 107 p28-36.